Title

In vivo detection of cortical optical changes associated with seizure activity with optical coherence tomography

Journal

Biomedical Optics Express, 3(11)

ISSN

2156-7085

Authors

Eberle, Melissa M
Reynolds, Carissa L
Szu, Jenny I
et al.

Publication Date

2012-11-01

DOI

10.1364/boe.3.002700

Peer reviewed

Biomedical Optics EXPRESS

In vivo detection of cortical optical changes associated with seizure activity with optical coherence tomography

Melissa M. Eberle,[1] Carissa L. Reynolds,[1] Jenny I. Szu,[2] Yan Wang,[1] Anne M. Hansen,[3] Mike S. Hsu,[2] M. Shahidul Islam,[1] Devin K. Binder,[2] and B. Hyle Park[1,*]

[1]*Department of Bioengineering, University of California, Riverside, 900 University Ave., Riverside, CA 92521, USA*
[2]*Division of Biomedical Sciences, University of California, Riverside, 900 University Ave., Riverside, CA 92521, USA*
[3]*Department of Statistics, University of California, Riverside, 900 University Ave., Riverside, CA 92521, USA*
**hylepark@engr.ucr.edu*

Abstract: The most common technology for seizure detection is with electroencephalography (EEG), which has low spatial resolution and minimal depth discrimination. Optical techniques using near-infrared (NIR) light have been used to improve upon EEG technology and previous research has suggested that optical changes, specifically changes in near-infrared optical scattering, may precede EEG seizure onset in *in vivo* models. Optical coherence tomography (OCT) is a high resolution, minimally invasive imaging technique, which can produce depth resolved cross-sectional images. In this study, OCT was used to detect changes in optical properties of cortical tissue *in vivo* in mice before and during the induction of generalized seizure activity. We demonstrated that a significant decrease ($P < 0.001$) in backscattered intensity during seizure progression can be detected before the onset of observable manifestations of generalized (stage-5) seizures. These results indicate the feasibility of minimally-invasive optical detection of seizures with OCT.

OCIS codes: (110.4500) Optical coherence tomography; (170.3880) Medical and biological imaging; (100.2960) Image analysis.

References and links

1. D. C. Hesdorffer, G. Logroscino, E. K. Benn, N. Katri, G. Cascino, and W. A. Hauser, "Estimating risk for developing epilepsy: a population-based study in Rochester, Minnesota," Neurology **76**(1), 23–27 (2011).
2. R. G. Andrzejak, D. Chicharro, C. E. Elger, and F. Mormann, "Seizure prediction: any better than chance?" Clin. Neurophysiol. **120**(8), 1465–1478 (2009), http://www.opticsinfobase.org/abstract.cfm?uri=BIOMED-2010-BSuD110p.
3. W. Stacey, M. Le Van Quyen, F. Mormann, and A. Schulze-Bonhage, "What is the present-day EEG evidence for a preictal state?" Epilepsy Res. **97**(3), 243–251 (2011).
4. L. Seungduk, J. L. Hyun, I. Changkyun, S. Hyung-Cheul, K. Dalkwon, and K. Beop-Min, "Simultaneous measurement of hemodynamic and neuronal activities using near-infrared spectroscopy and single-unit recording," J. Korean Phys. Soc. **58**(6), 1697–1702 (2011).
5. J. R. Weber, M. S. Hsu, A. Lin, D. Lee, C. Owen, D. K. Binder, D. J. Cuccia, W. R. Johnson, G. Bearman, A. J. Durkin, and B. J. Tromberg, "Noncontact imaging of seizure using multispectral spatial frequency domain imaging," in *Biomedical Optics*, OSA Technical Digest (CD) (Optical Society of America, 2010), paper BSuD110p.
6. D. K. Binder, M. C. Papadopoulos, P. M. Haggie, and A. S. Verkman, "In vivo measurement of brain extracellular space diffusion by cortical surface photobleaching," J. Neurosci. **24**(37), 8049–8056 (2004).
7. K. F. Rajneesh, A. J. Lin, J. J. Yeh, M. S. Hsu, and D. K. Binder, "Optical detection of the pre-seizure state in-vivo," J. Neurosurg. **113**(2), A422–A423 (2010).
8. K. Holthoff and O. W. Witte, "Intrinsic optical signals in vitro: a tool to measure alterations in extracellular space with two-dimensional resolution," Brain Res. Bull. **47**(6), 649–655 (1998).
9. A. S. Gill, K. F. Rajneesh, C. M. Owen, J. Yeh, M. S. Hsu, and D. K. Binder, "Early optical detection of cerebral edema in vivo," J. Neurosurg. **114**(2), 470–477 (2011).

#171757 - $15.00 USD Received 3 Jul 2012; revised 18 Sep 2012; accepted 26 Sep 2012; published 2 Oct 2012

10. J. M. Schmitt, "Optical coherence tomography (OCT): a review," IEEE J. Sel. Top. Quantum Electron. **5**(4), 1205–1215 (1999).
11. D. Huang, E. A. Swanson, C. P. Lin, J. S. Schuman, W. G. Stinson, W. Chang, M. R. Hee, T. Flotte, K. Gregory, C. A. Puliafito, and J. G. Fujimoto, "Optical coherence tomography," Science **254**(5035), 1178–1181 (1991).
12. Y. Satomura, J. Seki, Y. Ooi, T. Yanagida, and A. Seiyama, "In vivo imaging of the rat cerebral microvessels with optical coherence tomography," Clin. Hemorheol. Microcirc. **31**(1), 31–40 (2004).
13. M. Sato, D. Nomura, T. Tsunenari, and I. Nishidate, "In vivo rat brain measurements of changes in signal intensity depth profiles as a function of temperature using wide-field optical coherence tomography," Appl. Opt. **49**(30), 5686–5696 (2010).
14. A. D. Aguirre, Y. Chen, J. G. Fujimoto, L. Ruvinskaya, A. Devor, and D. A. Boas, "Depth-resolved imaging of functional activation in the rat cerebral cortex using optical coherence tomography," Opt. Lett. **31**(23), 3459–3461 (2006).
15. Y. Chen, A. D. Aguirre, L. Ruvinskaya, A. Devor, D. A. Boas, and J. G. Fujimoto, "Optical coherence tomography (OCT) reveals depth-resolved dynamics during functional brain activation," J. Neurosci. Methods **178**(1), 162–173 (2009).
16. U. M. Rajagopalan and M. Tanifuji, "Functional optical coherence tomography reveals localized layer-specific activations in cat primary visual cortex in vivo," Opt. Lett. **32**(17), 2614–2616 (2007).
17. J. F. de Boer, B. Cense, B. H. Park, M. C. Pierce, G. J. Tearney, and B. E. Bouma, "Improved signal-to-noise ratio in spectral-domain compared with time-domain optical coherence tomography," Opt. Lett. **28**(21), 2067–2069 (2003).
18. D. K. Binder, K. Oshio, T. Ma, A. S. Verkman, and G. T. Manley, "Increased seizure threshold in mice lacking aquaporin-4 water channels," Neuroreport **15**(2), 259–262 (2004).
19. S. H. Yun, G. J. Tearney, B. E. Bouma, B. H. Park, and J. F. de Boer, "High-speed spectral-domain optical coherence tomography at 1.3 μm wavelength," Opt. Express **11**(26), 3598–3604 (2003).
20. M. A. Choma, M. V. Sarunic, C. Yang, and J. A. Izatt, "Sensitivity advantage of swept source and Fourier domain optical coherence tomography," Opt. Express **11**(18), 2183–2189 (2003).
21. R. A. Leitgeb, W. Drexler, A. Unterhuber, B. Hermann, T. Bajraszewski, T. Le, A. Stingl, and A. Fercher, "Ultrahigh resolution Fourier domain optical coherence tomography," Opt. Express **12**(10), 2156–2165 (2004).
22. K. Bizheva, A. Unterhuber, B. Hermann, B. Povazay, H. Sattmann, W. Drexler, A. Stingl, T. Le, M. Mei, R. Holzwarth, H. A. Reitsamer, J. E. Morgan, and A. Cowey, "Imaging ex vivo and in vitro brain morphology in animal models with ultrahigh resolution optical coherence tomography," J. Biomed. Opt. **9**(4), 719–724 (2004).
23. Y. Wang, C. M. Oh, M. C. Oliveira, M. S. Islam, A. Ortega, and B. H. Park, "GPU accelerated real-time multi-functional spectral-domain optical coherence tomography system at 1300 nm," Opt. Express **20**(14), 14797–14813 (2012).
24. S. H. Yun, G. J. Tearney, B. E. Bouma, B. H. Park, and J. F. de Boer, "High-speed spectral-domain optical coherence tomography at 1.3 μm wavelength," Opt. Express **11**(26), 3598–3604 (2003).
25. K. K. Akula, A. Dhir, and S. K. Kulkarni, "Effect of various antiepileptic drugs in a pentylenetetrazol-induced seizure model in mice," Methods Find. Exp. Clin. Pharmacol. **31**(7), 423–432 (2009).

1. Introduction

Epilepsy, affecting at least 2% of the population [1], encompasses a group of disorders of the brain characterized by the periodic and unpredictable occurrence of seizures. As seizures are intermittent in patients with epilepsy, detection of seizures before they occur would be revolutionary in both warning patients and also developing "closed-loop" seizure detection and termination paradigms. To date, seizure detection algorithms have been solely based on analysis of either surface or intracranial electroencephalography (EEG). However, EEG has low spatial resolution, minimal depth discrimination and high susceptibility to electrical noise and motion artifacts. While great efforts are underway, there are currently no real-time methods of EEG analysis capable of reliably and reproducibly predicting seizure onset [2,3].

Optical techniques using near-infrared (NIR) light have been implemented to improve upon EEG technology by decreasing noise and increasing spatial and temporal resolution [4,5]. Previous research has suggested that optical changes, specifically changes in near-infrared optical scattering, may precede EEG seizure onset in animal models and that these optical changes are due to pre-seizure physiological changes, in particular reduction in the extracellular space [5–8]. Due to changes in the optical properties of the tissue, a decrease in intensity of backscattered light has been observed during the progression of seizures using noncontact NIR imaging and fiberoptic probes [5,7,9].

Optical coherence tomography (OCT) is a high resolution, minimally invasive, imaging technique which uses the short temporal coherence of a broadband light source to create

#171757 - $15.00 USD Received 3 Jul 2012; revised 18 Sep 2012; accepted 26 Sep 2012; published 2 Oct 2012

cross-sectional images in real time [10,11]. OCT has shown to be a promising method for *in vivo* imaging in highly scattering tissues such as the cerebral cortex and several groups have demonstrated that through functional OCT imaging, changes in tissue composition can be detected optically during stimulation [12–16]. In this study, we demonstrated that changes in the optical properties of brain tissue during the progression of seizures can be detected with the use of spectral-domain optical coherence tomography (SD-OCT) [17] by inducing a generalized seizure, measuring the changes in the backscattered intensity from the imaged tissue over time, and then quantifying these changes.

2. Materials and experimental methods

2.1 Animal preparation for in vivo experimentation

6-8 week old, CD1 female mice (25-35 g) were initially anesthetized intraperitoneally (i.p.) with a combination of ketamine and xylazine (80 mg/kg ketamine, 10 mg/kg xylazine) and anesthesia levels were carefully monitored via breathing rate and reflexes. A 4x4 mm thinned skull cortical window was created with a dental bur over the cerebral cortex. The skull was thinned to a uniform 55 µm. The mice were then imaged and a 10 min baseline was collected before a saline control injection was administered. After 25 to 30 min, pentylenetetrazol (PTZ) (100 mg/kg) was injected i.p. to induce a seizure. PTZ is a $GABA_A$ antagonist that reproducibly causes generalized seizures in this mouse model with a latency after injection [18], allowing for the study of the optical characteristics of the post-injection, pre-seizure state. Once a generalized tonic-clonic (stage-5) seizure was observed, involving fore- and hind-limb twitches and tail movement, the animal was sacrificed with an anesthesia overdose. All experimental procedures were approved by the University of California, Riverside Institutional Animal Care and Use Committee.

2.2 Spectral-domain optical coherence tomography (SD-OCT)

An SD-OCT system [17,19–21] optimal for imaging cortical tissue *in vivo*, utilizes a NIR light source centered at 1300 nm, providing an imaging depth of a few millimeters as well as achieving high spatial resolution [22]. The SD-OCT system we developed used a broadband, low-coherence light source consisting of two superluminescent diodes (SLD) centered at 1295 nm with a bandwidth of 97 nm, resulting in an axial and lateral resolution of 8 µm and 20 µm respectively. In our system, the source was split between a sample and reference arm with an 80/20 fiber coupler [23]. After recombination, the now interfered light was sent to a spectrometer where it was incident on a 1024 pixel InGaAs line scan camera (lsc) (Fig. 1).

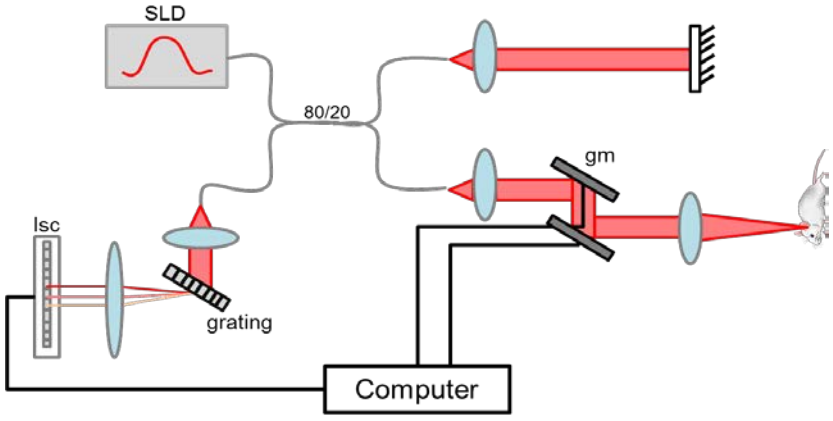

Fig. 1. Schematic of the SD-OCT system. SLD: superluminescent diode, lsc: line scan camera, gm: galvanometer.

#171757 - $15.00 USD Received 3 Jul 2012; revised 18 Sep 2012; accepted 26 Sep 2012; published 2 Oct 2012

2.3 Image acquisition and data processing

To image the mouse brain, we continuously scanned the motor cortex region of the right hemisphere centered over the corpus callosum. An imaging depth of 2 mm was obtained with 6 mW of incident power and a focal point 1 mm below the thinned skull. Axial line scans (A-lines) were acquired at 15 kHz, with each cross-sectional image consisting of 2048 A-lines spanning a 3 mm imaging plane. The spectral data was then sent to the graphics processing unit (GPU) where, to correct for the nonlinear *k*-space sampling interval, 512 sampled points per A-line scan were mapped to uniform frequency spacing by linear interpolation [24]. The GPU also handled the Fourier-transformation into the spatial domain and secondary image processing, including plotting the intensity images on a logarithmic inverse gray scale (Fig. 2) [23]. In SD-OCT, the sensitivity of the system decreases as a function of depth due to the finite resolution of the spectrometer and because of this, we applied a depth-correction function, reported by Yun *et al.* [24], during image processing by multiplying each A-line by the calculated correction curve. By applying the depth-correction, it also insured any change in tissue intensity was caused by biological effects not axial movement of the sample in the imaging window.

3. Results and discussion

3.1 Calculating average intensities from regions of interest

To analyze the changes in backscattered intensity resulting from changes in tissue composition during seizure progression, we calculated average intensities from regions of interest (ROI) over time. Our images had a maximum SNR of 45 dB above the noise floor and when selecting our ROIs we were careful to avoid regions where the SNR dropped below 10 dB. The ROIs we selected were approximately 1 mm deep and 3 mm wide and included all the cortical tissue in the imaging window because we were interested in the overall trend in intensity exhibited by the tissue. Minor variations in the ROI shape do not affect the final average intensity due to the high intensities of the selected regions (Fig. 2). To produce the results in Fig. 2, an image was analyzed every 10 s and the average intensities, which were normalized to the 10 min baseline, were plotted versus time. We also used a reference reflector during our experiments and analyzed small ROIs over time to ensure any changes were from biological phenomena and not system artifact.

3.2 Experimental controls

When designing our experiment, we used two controls. The first was a time sequence of baseline measurements, which were obtained prior to any experimental injection over the course of 10 min. The second was a saline injection with a volume equivalent to the PTZ dosage. This injection directly followed the baseline and post injection data was acquired for 25-30 min to establish if an injection alone causes a change in backscattered intensity from the imaged cortical tissue. In order to determine whether the saline injection caused any significant change in intensity, we calculated a two standard deviation (2SD) interval above and below the mean of the baseline spread and plotted the intervals in Fig. 2 to establish a high and low threshold for the intensity data. Due to low variability in the baseline data for all four experiments, we are able to construct narrow threshold intervals allowing us to detect even minor changes in intensity throughout experimentation.

It is apparent that there is no significant change in intensity during our controls (Fig. 2). To quantify our results, we calculated the baseline and post saline injection slopes through linear regression of the data in Fig. 2B for all four experiments. The intervals, from which the baseline slopes were calculated, began at time zero and ended at saline injection and the post saline injection slopes were calculated from the administration of the saline injection to PTZ injection. The average baseline slope was -0.16×10^{-3} NI/t and the average post saline injection slope was -0.59×10^{-3} NI/t. We used a Tukey multiple comparisons test to compare

#171757 - $15.00 USD Received 3 Jul 2012; revised 18 Sep 2012; accepted 26 Sep 2012; published 2 Oct 2012

baseline, post saline injection, and post PTZ injection slopes and our results indicated no significant change in intensity between baseline and post saline inj. with a *P*-value of 0.9997.

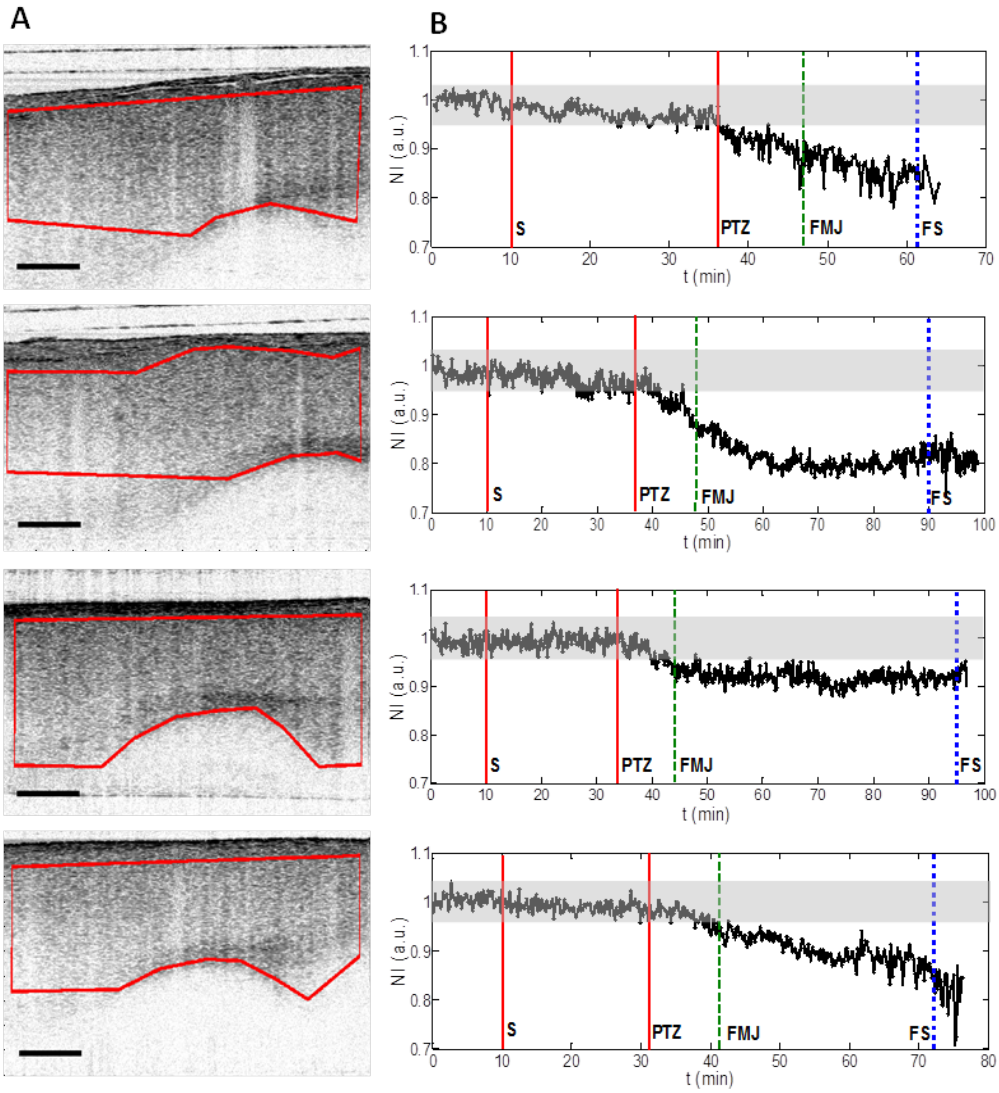

Fig. 2. Reduction in intensity during seizure progression. (A) OCT images of mice brain, one for each experiment, acquired *in vivo* with axial and lateral resolutions of 8 µm and 20 µm respectively. The red boxes indicate the ROIs used for average intensity calculations. The scale bar is 0.5 mm. (B) Plots of normalized intensity (NI) from the ROIs on left over time. The occurrences of the experimental steps are indicated: S: Saline injection (first red bar), PTZ: PTZ injection (second red bar), FMJ: Facial myoclonic jerks (green dashed line), FS: Full stage-5 seizure (blue dashed line). The gray region is the 2SD interval above and below the mean of the 10 min baseline.

3.3 Detection of optical changes during seizure progression

Directly after the saline control, we administered the PTZ injection to induce a seizure. OCT images were continuously acquired through the onset of a stage-5 seizure. The same ROI analysis was performed as was done for the controls and the resulting average intensities were plotted verses time in Fig. 2B. In all four experiments, a decrease in backscattered intensity

#171757 - $15.00 USD Received 3 Jul 2012; revised 18 Sep 2012; accepted 26 Sep 2012; published 2 Oct 2012

post PTZ injection was observed. This decrease from normal is due to the change in tissue composition, which precedes the onset of a seizure [6–8]. The average intensity in the ROI was monitored as it decreased below the 2SD threshold. Variability between when PTZ injection occurred and when the threshold was crossed in each experiment was due to the noise in the baseline spread from which the 2SD threshold was calculated (Fig. 3). Soon after the threshold was crossed, we observed facial myoclonic jerks (FMJs) (Fig. 2), which are events associated with the early stages of seizure progression [25]. The timing from when the threshold was crossed to when the FMJs were observed varied between experiments, ranging from 1 to 10 min. However, the threshold crossing always occurred at least a minute before the first observed FMJs. This indicated that a significant decrease in intensity from baseline can be detected with OCT before the onset of observable physical manifestations associated with early stages of seizures. Also, because of the narrow threshold interval, we detected a significant decrease in intensity, even in the experiments where the total percent decrease from baseline was under 10%.

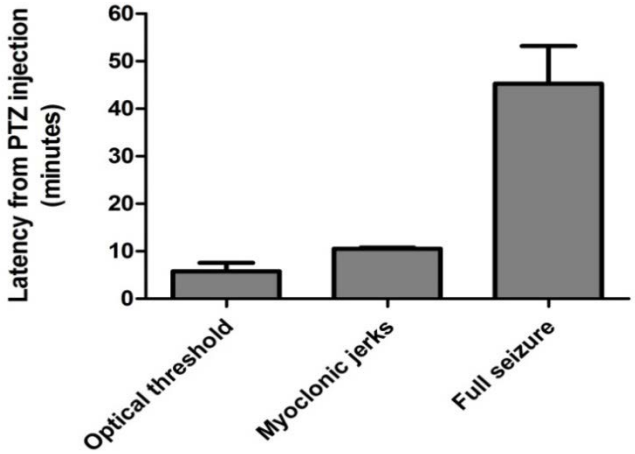

Fig. 3. OCT-detected "optical threshold" precedes myoclonic jerks and full seizure. Latency from PTZ injection (min) displayed for optical threshold (defined as 2SD change in intensity), myoclonic jerks, and full stage-5 (generalized tonic-clonic) seizure. Optical threshold crossing preceded both myoclonic jerks (focal seizure) and generalized seizure, indicating the ability of OCT to optically detect pre-seizure state.

3.4 Analysis of changes during experimental steps

We imaged through the initiation of a stage-5 seizure, which due to the variability in anesthesia levels occurred at different time points after PTZ injection (Fig. 3). As the seizures progressed, the intensity from the imaged areas continued to decrease. To quantify the changes in intensity, we calculated the slopes post PTZ injection for each of the four experiments using linear regression. The intervals for the slope calculations began at PTZ injection and ended once the data began to deviate from the linear decreasing trend. We then averaged the four slopes and plotted them in Fig. 4 along with the baseline and post saline injection average slopes. The interval bars in Fig. 4 were calculated by a 90% confidence interval (C.I.) using the t-distribution for small sample sizes. The average slopes and intervals for each of the three experimental steps were: baseline $-0.16 \times 10^{-3} \pm 0.99 \times 10^{-3}$ NI/t, post saline inj. $-0.59 \times 10^{-3} \pm 0.81 \times 10^{-3}$ NI/t, and post PTZ inj. $-5.3 \times 10^{-3} \pm 1.99 \times 10^{-3}$ NI/t.

The differences in the slopes between experimental steps were analyzed with an ANOVA F-test and the results are summarized in Table 1. Even with slope variability between the four experiments, there is a significant difference between the treatments ($P < 0.001$), indicating that the mean slopes for all three steps are not equal.

#171757 - $15.00 USD Received 3 Jul 2012; revised 18 Sep 2012; accepted 26 Sep 2012; published 2 Oct 2012

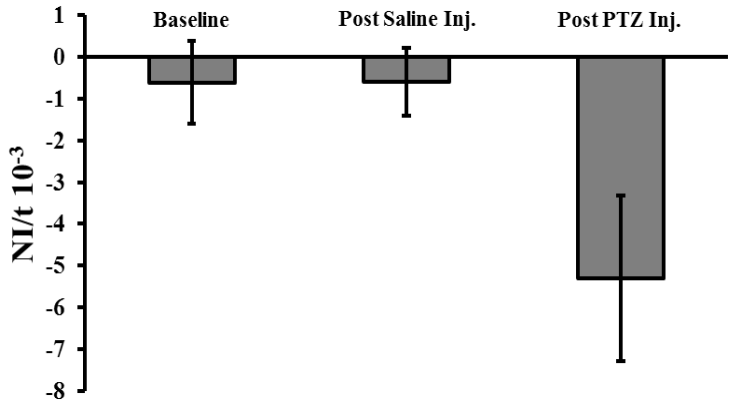

Fig. 4. Plot of the three average slopes: Baseline, Post saline injection, and Post PTZ injection. The average slopes were calculated from four seizure experimental data sets. The interval bars were calculated with a 90% confidence interval using the t-distribution. NI: Normalized Intensity, t: time (min), Inj.: Injection.

Table 1. ANOVA for the average slopes of the three experimental steps

	df	Sum of Square	Mean of Square	F-value	*P*-value
Treatment	2	5.98×10^{-5}	2.99×10^{-5}	22.34	1×10^{-4}
Error	9	$1.2. \times 10^{-5}$	1.34×10^{-5}		

df: degrees of freedom

To explore the differences found with the ANOVA F-test, we performed a Tukey multiple comparisons test to compare the baseline, post saline, and post PTZ slopes. As mentioned previously in Section 3.2, the baseline and post saline slopes were not significantly different. This procedure also compared the post PTZ injection slopes to the baseline and post saline injection slopes. The resulting *P*-values were $P < 0.001$ for both comparisons: post PTZ injection slope to the baseline slope and post PTZ injection slope to the post saline injection slope. This demonstrates that the change in backscattered intensity as a seizure progresses can be quantified and when compared with pre-seizure states, signifies that there is a significant decrease in intensity, detectable with OCT.

4. Conclusion

In conclusion, we conducted seizure experiments *in vivo* to establish, as a proof of principle, that a decrease in intensity during seizure progression can be detected through OCT imaging. We created a threshold interval model for the temporal identification of changes in the backscattered intensity. Our results indicated that crossing below the definable optical detection threshold occurred prior to either FMJs or generalized (tonic-clonic) manifestations of seizure activity. In the future, we plan on further developing this into an optical trigger to help identify the occurrence of seizures prospectively even before physical manifestations are present. These results could lead not only to optical seizure detection but also prediction with appropriate algorithmic real-time analysis of the OCT signal. Furthermore, previous research has used OCT to spatially resolve changes in cortical tissue during electrical stimulation [14,15] and by utilizing the high spatial and temporal resolution of OCT, it will be possible to map changes in intensity during seizure progression and propagation through the intact brain.

Acknowledgments

The authors acknowledge financial support from the following US National Institutes of Health grants: R00EB007241, and K08NS059674.

#171757 - $15.00 USD Received 3 Jul 2012; revised 18 Sep 2012; accepted 26 Sep 2012; published 2 Oct 2012